Nanoscale

COMMUNICATION

View Article Online
View Journal

Cite this: DOI: 10.1039/c5nr03762j

Received 8th June 2015,
Accepted 8th October 2015

DOI: 10.1039/c5nr03762j

www.rsc.org/nanoscale

Nano-scale, planar and multi-tiered current pathways from a carbon nanotube–copper composite with high conductivity, ampacity and stability

Chandramouli Subramaniam,*[a] Atsuko Sekiguchi,[b] Takeo Yamada,[b] Don N. Futaba[b] and Kenji Hata*[b]

New lithographically processable materials with high ampacity are in demand to meet the increasing requirement for high operational current density at high temperatures existing in current pathways within electronic devices. To meet this demand, we report an approach to fabricate a high ampacity (~100 times higher than Cu) carbon nanotube–copper (CNT–Cu) composite into a variety of complex nano-scale, planar and multi-tiered current pathways. The approach involved the use of a two-stage electrodeposition of copper into a pre-patterned template of porous, thin CNT sheets acting as the electrode. The versatility of this approach enabled the realization of completely suspended multi-tier, dielectric-less 'air-gap' CNT–Cu circuits that could be electrically isolated from each other and are challenging to fabricate with pure Cu or any metal. Importantly, all such complex structures, ranging from 500 nm to 20 μm in width, exhibited ~100-times higher ampacity than any known metal, with comparable electrical conductivity as Cu. In addition, CNT–Cu structures also exhibited a superior temperature stability compared to the ~10-times wider Cu counterparts. We believe that the combination of our approach and the properties demonstrated here are vital achievements for the future development of efficient and powerful electrical devices.

Introduction

Rapid advancements in electronics have been realized following the paradigms of Moore's law and miniaturization.[1] The paradigm of Moore's law has led to more devices and components being operated in increasingly confined spaces.[2] This creates energy localizations, where devices operate under extreme conditions, such as high temperature and high current density.[3] This imposes severe operating conditions on the electrical pathways to, from, and within these energy localizations, with the demand rapidly approaching the maximum current-carrying-capacity (*i.e.* ampacity) limits of metals.[4] In fact, the International Technology Roadmap for Semiconductors (ITRS) estimates that the current density in devices will exceed the ampacities of Cu and Au (~10^6 A cm^{-2}) by 2015.[5] Therefore, an alternative electrical conductor with high ampacity in addition to a reliable performance at high temperatures is in immediate demand.

Electro-migration and the resulting thermal-migration are the primary mechanisms limiting the performance of metals at high current densities and high temperatures.[6] Electro-migration refers to the migration and mass-transport of atoms of conducting elements, induced by a large current density and is prominent in metallic conductors such as Cu, Al and Au due to their loosely bound metallic bonds.[6] This simultaneously increases the temperature of the conductor by Joule heating, leading to thermal-migration and consequent failure.[7] In contrast, a strong covalent bond of carbon materials, such as carbon nanotubes[8] (CNTs) and graphene,[9] provides a much higher ampacity (10^8–10^9 A cm^{-2}). However, the discrete density of states results in lower conductivity when compared to metals such as Cu and Au.[8,9] Therefore, avoiding these two failure pathways is of significant scientific and technological interest for the development of electronic devices.

A promising approach is to synergistically combine CNT and Cu while preserving the strengths (ampacity and conductivity respectively) of each material. It has been demonstrated that making a CNT–Cu composite could combine the strengths of both Cu and CNTs.[10] We recently demonstrated the fabrication of a CNT–Cu composite which exhibited comparable electrical and thermal conductivity as pure Cu while possessing a 100-fold higher ampacity than Cu[10] and a coefficient of thermal expansion (CTE) close to Si.[11] While these properties of a bulk CNT–Cu composite are very promising, the key challenge for the material to be used in devices is to establish its processability and patternability into lines and circuits,

[a]*Technology Research Association for Single Wall Carbon Nanotubes (TASC), Currently at Department of Chemistry, Indian Institute of Technology Bombay, Powai, Mumbai 400076, Maharashtra, India. E-mail: csubbu@chem.iitb.ac.in*
[b]*Nanotube Research Center, National Institute of Advanced Industrial Science and Technology (AIST), Central 5, 1-1-1 Higashi, Tsukuba 305-8565, Japan. E-mail: kenji-hata@aist.go.jp*

through methods that are compatible with the existing semiconductor techniques while simultaneously preserving the properties of the bulk CNT–Cu composite.

Addressing this challenge, we report a strategy to achieve complex nano-dimensional patterning with the CNT–Cu composite. Our approach is based on the combination of the transfer of self-supporting, thin, aligned CNT sheets to a substrate; patterning them into arbitrary shapes, and then using them as porous electrodes for Cu electrodeposition. This strategy enabled the fabrication of a CNT–Cu composite with nanoscale features with various sizes and shapes. Importantly, the patterned CNT–Cu features showed similar electrical conductivity (2.5×10^5 S cm^{-1}) and ampacity (5.5×10^8 A cm^{-2}) as the bulk material reported previously (4.5×10^5 S cm^{-1}, 6×10^8 A cm^{-2}, respectively).[10,11] We would like to emphasize that the fabrication method, for this material, is compatible with conventional semiconductor processes as the CNT-sheet transfer step is carried out at room temperature and thus is completely isolated from the high-temperature CNT synthesis. Besides, the maximum temperature employed during the thermal reduction step (250 °C) is much lower than what large-scale integrated circuits can withstand.

Experimental and methods

Materials

Aligned CNT sheets were synthesised using the water-assisted super-growth chemical vapor deposition (CVD) technique from patterned Fe catalysts.[12] Briefly, CNTs were synthesized from Al_2O_3 (40 nm)/Fe (1.5 nm) catalysts sputtered on silicon wafers with C_2H_4 (100 sccm) as the carbon source and water (100 to 150 ppm) as the oxygen source. The synthesis was carried out at 750 °C on a fully-automated CVD furnace. The forest consisted of aligned, single-walled carbon nanotubes (CNTs, diameter ~2.8 nm) with high purity (99%).[12] All other chemicals were purchased from Wako and used without further purification, unless specified otherwise.

Results and discussion

The fabrication of the CNT–Cu composite pathways consists of the following major fabrications steps, as shown in Fig. 1(a). Our approach is based on the combination of the transfer of self-supporting, thin, aligned CNT sheets to a substrate; patterning them into arbitrary shapes, and then using them as porous electrode templates for Cu electrodeposition. First, aligned SWNT sheets (1 mm width, ~8 μm thickness and 1 mm long; CNT diameter ~3 nm) were synthesized by water-assisted chemical vapor deposition (CVD) from patterned Fe catalysts.[12] Second, the CNT sheets were transferred onto a Si wafer (SiO_2 thickness ~100–500 nm), and densified into a closely packed, aligned CNT 'wafer' (0.5 g cm^{-3}, ~1 mm long).[13] Third, the CNT wafer was lithographically patterned into the desired configurations in a manner† analogous to that in Si processing.[13] Fourth, the copper was galvanostatically deposited into the pores of the CNT film patterns to form

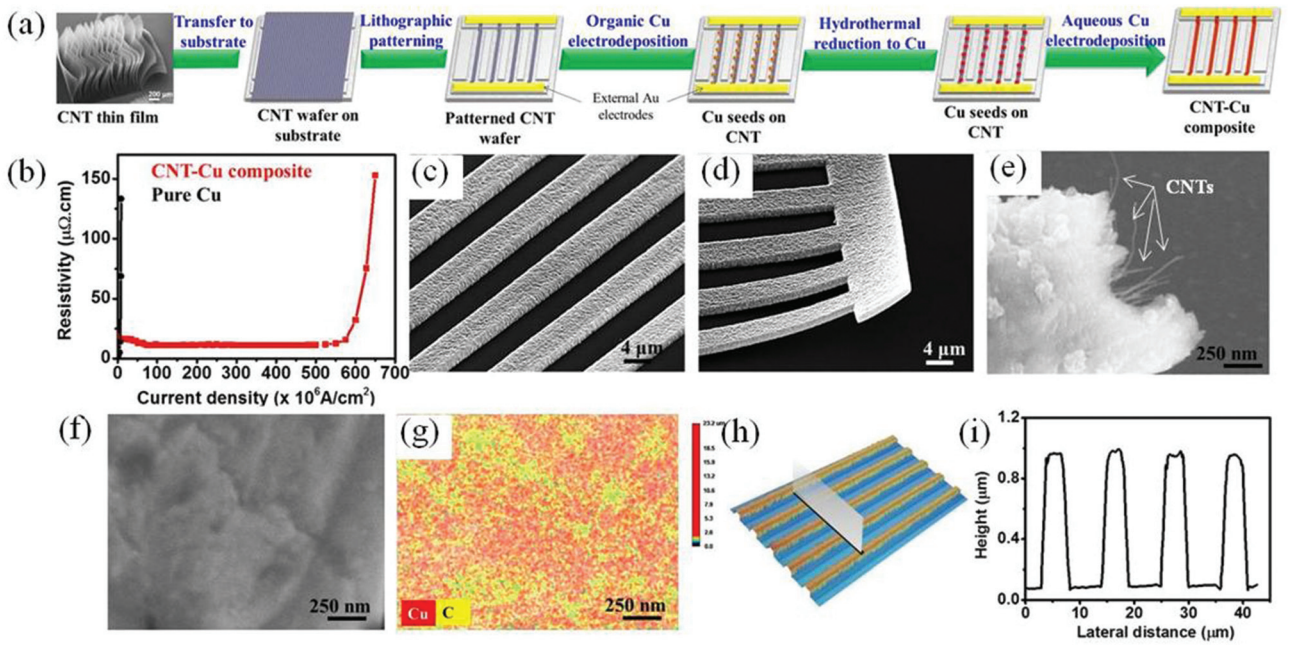

Fig. 1 (a) Schematic representation of the strategy developed for achieving sub-micron features of the CNT–Cu composite. (b) Plot of resistivity *versus* current density for the CNT–Cu composite (red trace) and Cu (black trace) confirming an ~100 times higher ampacity for nano-scale CNT–Cu current pathways. (c) Periodic two-dimensional current pathways with the CNT–Cu composite. (d) A delaminated section of the patterned CNT–Cu composite showing structural cohesiveness and integrity. (e) and (f) represent the SEM of a fractured cross-sectional surface of the CNT–Cu composite with (g) presenting the EDX mapping based on Cu (red) and C (yellow). (h) Confocal laser scanning microcopy image of the CNT–Cu current pathways with the height profile shown in (i).

seeds by electrodeposition using an organic electrolyte (27.7 mM $Cu(CH_3COO)_2$ in CH_3CN). The similarity in solubility parameters of acetonitrile (18 $MPa^{1/2}$) and CNTs (18.6 $MPa^{1/2}$) allowed homogeneous deposition of Cu seeds.[14] Fifth, thermal reduction of the Cu seeds was performed (250 °C, H_2 flow rate of 150 sccm, 3 h) to remove the oxide. Finally, Cu filling by aqueous electrodeposition was applied to complete the filling of Cu ions. The ampacity was measured on such nanoscale, conductive CNT–Cu lines and was estimated to be 5.5×10^8 A cm^{-2} with the highest being 5.7×10^8 A cm^{-2}, close to a hundred times higher than that measured on copper of identical dimensions (Fig. 1(b)). The CNT interstitial spaces were completely filled with copper as shown by the fractured cross-section of a pathway (Fig. 1(e) and (f)). In fact, the continuous nature of the CNT–Cu medium could be evidenced from the unfractured, de-laminated pathways (Fig. 1(d)). Secondary electron microscopy (SEM, Fig. 1(c)) and cross-sectional line-profiles (Fig. 1(i)) by confocal laser scanning microscopy (Fig. 1(h)) recorded in the same position of the sample confirmed the height and width uniformity (1 μm thick, 4 μm width) between each conductive pathway. The microstructure of the composite exhibited good homogeneous distribution of carbon and copper as seen from energy-dispersive X-ray (EDX) analysis (Fig. 1(g)). Higher magnification imaging showed evidence of extensive interfacing between the CNTs and Cu at length-scales as low as a few nanometers (~10 nm).

Electrical characterization revealed that the conductivity and ampacity of the macroscopic-scale composite carried over to the micro-patterned CNT–Cu pathways (1 μm thick, 4 μm wide). Room temperature 4-probe measurements showed an electrical conductivity of 2.5×10^5 S cm^{-1}, similar to 4.5×10^5 S cm^{-1} for bulk CNT–Cu.[10,11] Next, we measured the ampacity of these nano-scale structures by passing direct current through several individual line structures (0.5 μm wide, 1 μm thick) and found an average ampacity of 5.5×10^8 A cm^{-2} with the highest being 5.7×10^8 A cm^{-2} (Fig. 1(b)). This value is ~100 times higher than any metal (Cu, Au: ~10^6 A cm^{-2}) and consistent with our earlier report.[10] It should be noted that the coefficient of thermal expansion (CTE) of the bulk CNT–Cu was measured to be similar to that of silicon (~1/5th that of copper), which is ideal for interfacing with silicon-based platforms.[11,15] This aspect would be vital for applications such as through-silicon vias where the thermal expansion mismatch between the conductor and the substrate is a significant problem.[15]

We found that the filling of the CNT interstitial spaces with Cu becomes particularly difficult when the macroscopic CNT structure is large or densely packed. Once the Cu is deposited into the interstitial spaces, the migration pathways for Cu^{2+} ions become smaller, thereby increasing the difficulty to fill the entire CNT material. In the current work, the density of thin CNT wafers was 0.5 g cm^{-3}, meaning the CNT occupied ~50% of the volume. This high density was required to able to coat resist on the CNT wafer in order to apply standard lithography. We believe that the small physical dimensions of the pathways allowed for sufficient diffusion to deposit Cu throughout the CNT material. From this point, we could fabricate pathways with a width down to 500 nm (Fig. 2(d)). Therefore, we believe that further dimensional down-scaling is feasible for the composite as the Cu diffusion is facilitated by smaller template (CNT wafer) dimensions.

Our approach toward the fabrication of highly electrically conductive CNT–Cu pathways was extended to the fabrication of complex patterns. The CNT pattern was designed to possess an aggregate cross-sectional area approximately constant at any location between the two electrodes. In this manner, the current density passing through each segment, big or small, of the CNT pattern was kept constant, and thus Cu could be deposited uniformly. This allowed fabricating structures with arbitrary combinations of filling ratios, uniformity, and homogeneity, provided the condition of a constant aggregate cross-sectional area was satisfied. As demonstrated, structures with significantly different dimensions, ranging from 500 nm to 5 μm, could coexist in directions both parallel and perpendicular to the electrodes across wide areas (Fig. 2(a)). A combination of basic structures, such as bends and junctions, could be used to fabricate unique H-, L- and Z-shaped architectures with the CNT–Cu composite (Fig. 2(f)–(i)). Structures of varying sizes could also be fabricated, as shown by the islands distributed throughout the pattern; moreover, these islands co-existed with thin pathways, which could be fabricated from the same CNT film. The smallest feature fabricated was ~500 nm wide, uniform, and homogeneous (Fig. 2(d)) and could be simultaneously fabricated with the much larger structures (Fig. 2(h)). Elemental mapping by EDX indicates the presence of both Cu and C, distributed evenly along the patterns, across a wide area of the sample (Fig. 2(b)). Minor variations in the intensity distribution are attributed to the orientation of the sample during the EDX mapping. Confocal microscopy images showing the cross-section of various features (ranging from widths of 500 nm to 5000 nm) indicate similar heights, which is evidence that each CNT pattern was deposited with a similar amount of copper, and, therefore formed an identical composite (Fig. 2(c) and (e)). Our results imply that designing suitable external electrodes would enable the fabrication of a diverse variety of patterns.

The flexibility of the CNTs and the cohesiveness of the film allowed the extension of this approach to the fabrication of structures not possible through standard silicon based fabrication processes: suspended, three-dimensional (3-D) current pathways.[16] To this end, the CNT wafer was fabricated over a Si wafer with pre-patterned silicon pillars (1 μm^2 area, 1.5 μm height) resulting in a 3-D CNT wafer that seamlessly traversed the substrate plane and elevated planes (Fig. 3(c)). The CNT wafer could then be etched to form alternating suspended, bi-planar and planar pathways and be subsequently converted into the composite by electrodeposition (Fig. 3(e)). In order to demonstrate the uniform electrical properties of these bi-planar lines, *I–V* traces across CNT–Cu structures made with Si pillars of three different heights (0 μm, 1.25 μm, and 2.5 μm) were measured and found to be identical (Fig. 3(a)). As seen from the SEM (Fig. 3(b)–(e)) and confocal microscopy imaging

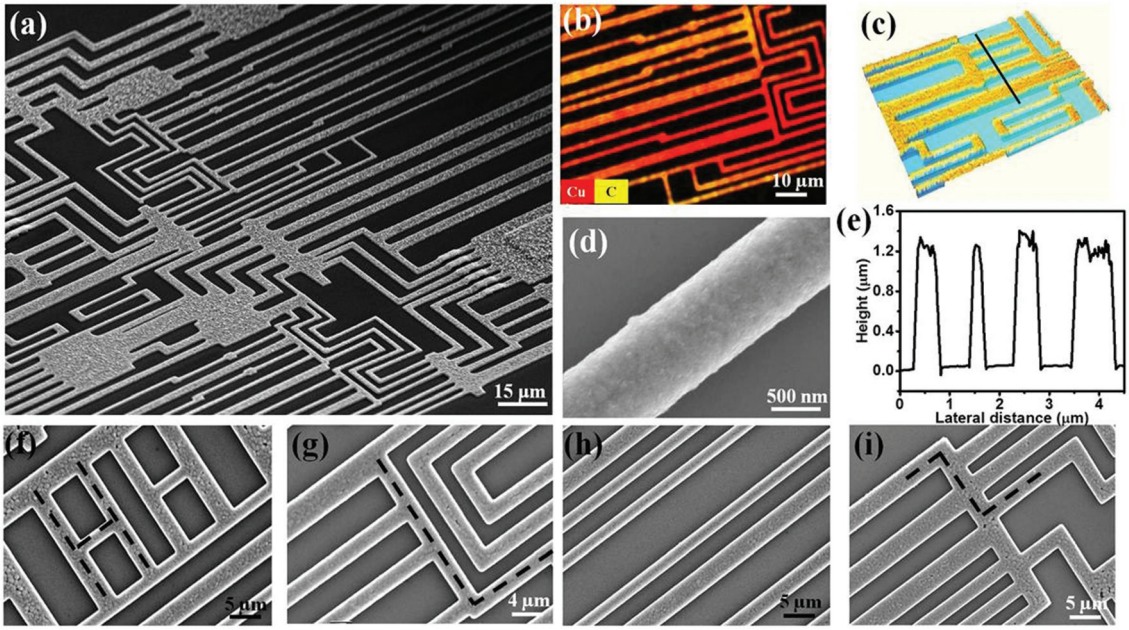

Fig. 2 (a) SEM image of a complex combination of CNT–Cu current pathways consisting of arbitrary shapes and dimensions fabricated over an area of ~2500 μm^2 in a single batch. (b) EDX elemental mapping (based on Cu and C) of such complex combinations of current pathways. (c) Confocal laser scanning microscopy image of a portion of such patterned structures. The height profile obtained across the black line indicated is given in (e) showing the uniform height of the CNT–Cu composite patterns, irrespective of their differing widths (500 nm to 1.5 μm). (d) SEM image of an isolated nano-dimensional CNT–Cu conductor showing the uniformity of the material. SEM images of several nano-scale structures with configurations such as H-shaped, L-shaped, S-shaped and their combinations thereof are presented from (f) to (i).

(Fig. 3(f)), the height profile across these alternating patterns (Fig. 3(g), red trace) also alternates between ~1 and 2 μm, indicating a uniformly thick composite (~1 μm) for both planar and bi-planar current pathways. Furthermore, line profiles taken along a single bi-planar structure showed a seamless height transition from 0.3 μm to 1.25 μm (Fig. 3(g), black trace). As the height of the pillar was 1 μm, this further demonstrates that we were able to make a uniform material in a bi-planar configuration. These aspects demonstrated the feasibility of our approach to fabricate bi-planar CNT–Cu structures as reliable current pathways.

The potential to fabricate 3-D CNT–Cu architectures could be further extended to make multi-tiered pathways using the strategy outlined (Fig. 4(a)). An entire CNT film was suspended on silicon pillars (1.5 μm height) to form the top tier over a series of prefabricated Au pathways representing the bottom

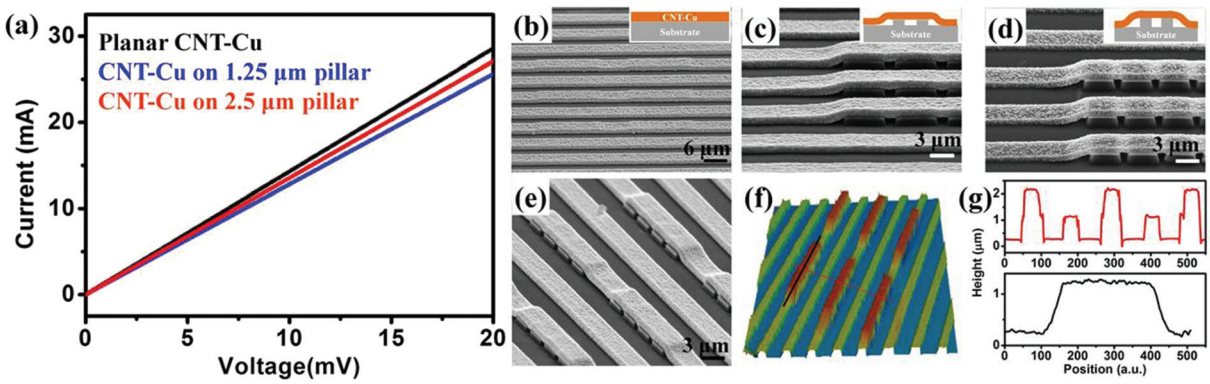

Fig. 3 (a) *I*–*V* traces of two-dimensional, planar and three-dimensional, bi-planar CNT–Cu structures fabricated over Si pillars of different heights. SEM images of multi-dimensional CNT–Cu current pathways that seamlessly traverse across different heights are given in (b) to (d). The heights of the Si pillars are 1.25 μm and 2.5 μm in (c) and (d), respectively. (e) SEM image of alternating planar and bi-planar current pathways fabricated with the CNT–Cu composite. (f) Confocal laser scanning microscopy image of the pattern in (e). The height profiles across the black and red lines on the image are provided in (g) and confirm the uniformity of the CNT–Cu composite pathways extending in multiple dimensions.

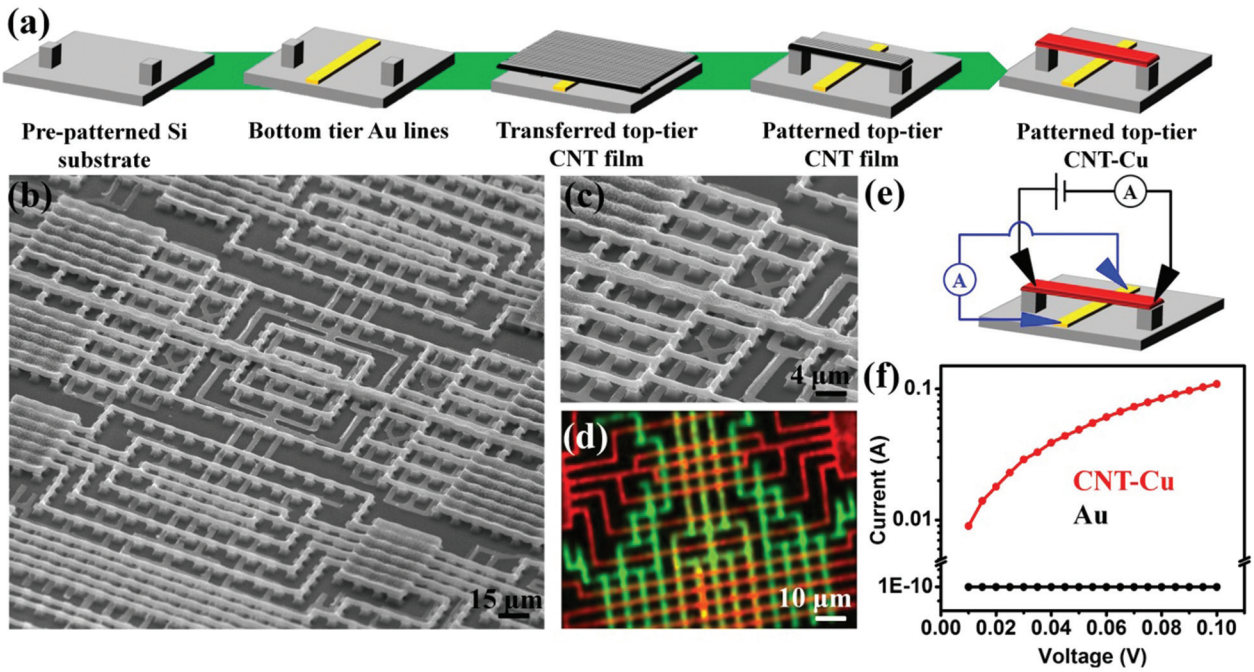

Fig. 4 (a) Schematic representation of the fabrication of multi-tier, air-gap circuits with the CNT–Cu composite. (b) SEM image of the CNT–Cu composite, air-gap circuits showing the dielectric-less air-gap between the top tier of the CNT–Cu composite and bottom tier Au lines. (c) The physical separation of the two tiers is seen in the SEM image. (d) EDX mapping of such air-gap separated circuits, based on Cu (red) and Au (green), reveals the absence of a physical overlap between the two tiers. This is further confirmed from electrical measurements, the schematic and the data of which are presented in (e) and (f), respectively.

tier. The suspended CNT sheet in the top tier was etched into patterns and subsequently converted into CNT–Cu by electrodeposition. Such three-dimensional CNT–Cu structures could be fabricated into versatile shapes and sizes (Fig. 4(b)) despite being completely suspended with the widths of the lines varying from 1.5 μm to 5 μm (thickness ~1 μm). A variety of complex, fully suspended current pathways were then fabricated to include branching patterns comprising of both orientations (parallel and perpendicular) of aligned CNTs (Fig. 4(c)). The distance between the bottom Au tier and the top CNT–Cu tier was estimated to be ~1.3 μm from the SEM images (Fig. 4(c)) which corresponded well with the height of the pillars. Further, electrical isolation between the two tiers was confirmed using the schematic in Fig. 4(e). A potential difference was applied across the top tier, consisting of CNT–Cu and the current was measured across the bottom tier. A negligible leakage current ($\sim 10^{-10}$ A, close to the resolution of the measurement system) was measured, demonstrating the electrical isolation between the upper and lower tiers (Fig. 4(f)). This was also confirmed through EDX elemental mapping that showed clear elemental separation of the bottom Au tier and the CNT–Cu pathways in the top-tier. Since, deposition of Cu on CNT proceeded through the creation of an electric field, any physical contact of CNT (top-tier) with Au (bottom tier) would have resulted in Cu being deposited on Au lines as well. Therefore, the observation of distinct EDAX signatures from both Au and Cu, without any mixing, confirms that CNT–Cu is physically separated from the Au tier. That is, the absence of the Cu signals on the Au lines is evidence of specific electrodeposition on the CNT lines, confirming electrical isolation between tiers (Fig. 4(d)). Our multi-tier pathways can be considered as "air-gap" circuits, with vacuum as a dielectric medium between the metallization lines providing the ideal dielectric separation between them.[17] Such multi-tier architectures can be used to address the parasitic capacitance occurring in closely-spaced metallization lines.[17]

In order to investigate the stability of our CNT–Cu pathways, we implemented lifetime evaluation at high current densities (10^7–10^8 A cm^{-2}) and temperatures (250 °C) that Cu cannot withstand (Fig. 5(a)). The mean time to failure was defined as the point of 20% decrease in conductivity and was determined for two line-widths of the CNT–Cu composite (500 nm and 5000 nm).[18] Both the CNT–Cu composite and Cu showed a similar behaviour, where at the initial stages the conductivity was stable, while beyond a particular time it dropped exponentially and failed. In all cases, the CNT–Cu composite showed a significantly longer lifetime, highlighting its superiority over Cu. The lifetime was estimated and plotted as a function of current density (Fig. 5(b)). Both the CNT–Cu composite and Cu showed a monotonic decrease in their lifetimes as the current density increased, with the CNT–Cu structures always possessing a significantly longer lifetime. In particular, the CNT–Cu structures with a 500 nm width exhibited a longer lifetime than a 10-fold wider pure copper line

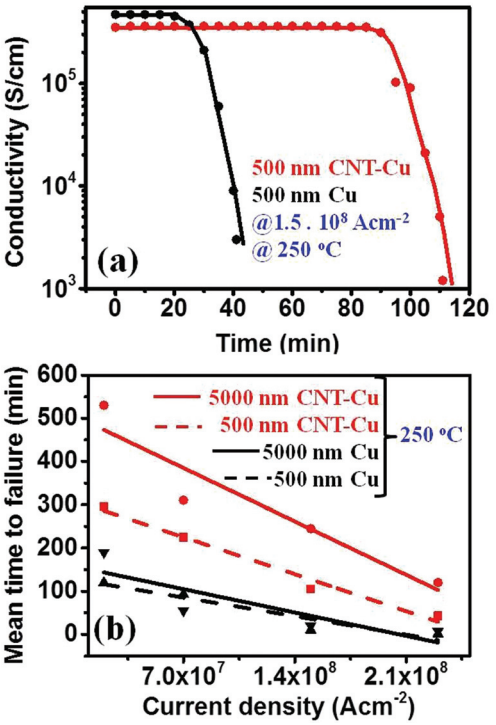

Fig. 5 (a) Time-evolution of electrical conductivity of the CNT–Cu composite (red) and Cu (black) under stress conditions of 1.5×10^8 A cm^{-2} and 250 °C. (b) Plot of mean-time-to-failure for the CNT–Cu composite and Cu structures of two different dimensions (500 nm and 5000 nm width) showing a significantly superior lifetime and stability of the CNT–Cu composite.

(5000 nm) (Fig. 5(b)). This result implies that a 10-fold decrease in line-width is possible by replacing Cu with CNT–Cu.

Although the mechanism of the high performance of the CNT–Cu lines is not yet completely well understood, theory predicts that carbon-doping into Cu would increase the activation energy of diffusion of Cu.[10,19] The two primary mechanisms acting to achieve this are dopant-dragging[19] (migration of Cu with C, resulting in an increase in activation energy) and dopant-blocking[19] (occupancy of Cu interstitial sites by carbon, resulting in physical obstruction of the migration pathways). We expect the CNTs to act similar to the dopant carbons; however CNTs themselves possess a very high tolerance to electromigration. Therefore, the dopant dragging mechanism is expected to be less dominant here. Thus, we expect that CNTs are blocking and suppressing Cu diffusion to yield a higher ampacity and a more stable conducting composite.

Conclusions

In conclusion, we demonstrated an approach to fabricate the nano-scale patterning of a CNT–Cu composite possessing electrical conductivity on par with Cu and ampacity ~100 times higher than Cu. Through the use of an aligned CNT sheet as a porous electrode, Cu could be uniformly electrodeposited throughout the patterned sheet to create a homogeneous micropatterned CNT–Cu composite. Complex bi-planar and multi-tiered, electrically isolated air gap structures could be fabricated, which are otherwise impossible by the conventional vapor deposition of Cu, thereby illustrating the strength of this approach. Importantly, the electrical conductivity and ampacity carried over from the macroscopic dimensions to the submicron structures. Taking these results together, we believe that sustaining the properties at nanoscale dimensions as demonstrated here provides a feasible approach for utilization of CNT–Cu electrical current pathways in electronic devices.

Acknowledgements

This paper is based on results obtained from a project commissioned by the New Energy and Industrial Technology Development Organization (NEDO). C.S., T. Y. and K.H. devised the experiments, C.S. and A.S. performed the experiments, C. S. D. N.F. and K.H. co-wrote the paper, K. H. designed and supervised the project.

Notes and references

† *Patterning of the CNT film*

Vertically aligned CNT sheets (measuring 700 μm × 700 μm with an as-grown thickness of 8 μm) were carefully transferred to the desired substrate in the desired orientation using a liquid-induced densification approach.[13] The CNT sheets were then transferred from the growth substrate to the target substrate. Although such CNT sheets were sparse (~0.04 g cm^{-3}), the long and entangled CNTs provided them with sufficient mechanical cohesiveness to allow their handling as a continuous unit for removal and transfer without damage. Thus, such CNT sheets were transferred onto a Si wafer (SiO_2 thickness ~100–500 nm), and densified into a closely packed, aligned CNT 'wafer' (0.5 g cm^{-3}, ~1 mm long) using a liquid-induced densification approach as previously described.[13] The thickness of the CNT films after attachment to the substrate was measured to be around 700 nm. Then, the CNT wafer was patterned into desired configurations.

Positive tone PMMA-495 (Microchem Corp.) was spin coated at 4700 rpm for 60 s on the substrate followed by curing at 180 °C for 60 s. A double mask recipe was adapted using a negative tone FOX 16 (flowable oxide, Dow Corning) on top of the cured PMMA-495. The FOX 16 was spin coated at 4500 rpm for 60 s followed by baking at 120 °C for 8 minutes. Electron-beam lithography was used to expose the required areas of CNTs. The substrate was developed using tetramethylammonium hydroxide (TMAH), rinsed with water and dried under a dry N_2 flow. Reactive ion etching (RIE) using a mixture of O_2/Ar /CHF_3 was carried out to remove the unwanted CNT areas. After the CNT patterning, the negative resist and positive resist were removed using buffered hydrogen fluoride (BHF) and a 1 : 1 mixture of methylisolbutyl ketone/isopropyl alcohol (MIBK/IPA), respectively. Finally, the subtrate was rinsed in IPA and dried under a N_2 stream before Cu electrodeposition.

Microfabrication of CNT–Cu composite

Metal electrodes (3 nm Ti and 100 nm Au) were fabricated by sputtering on the Si or Si_3N_4 substrates after defining the required shapes through electron beam lithography. The CNT sheets were transferred from the growth substrate to the target substrate using the liquid-induced densification approach[13] and oriented in the desired alignment.

Copper was deposited into the pores of the CNT film patterns to form seeds by electrodeposition. Despite being densified, these patterned CNT wafers were

sufficiently porous (~50%) to allow deposition of Cu onto all CNT surfaces, both on the periphery and in the pore volume of the wafers, to make a CNT–Cu composite that was homogeneous enough to act as a single cohesive unit. Thermal reduction of the Cu seeds was performed (250 °C, H_2 flow rate of 150 sccm, 3 h) to remove the oxide and other organic contaminations. Finally, Cu filling by aqueous electrodeposition was applied to complete the filling of Cu ions into the porous CNT template with a high (55 vol%) and homogeneous filling of Cu.

1 U.S. Congress, Office of Technology Assessment, Miniaturization Technologies, OTA-TCT-514, U.S. Government Printing Office, Washington, DC, November, 1991.
2 G. E. Moore, *Proc. IEEE*, 1998, **86**, 82.
3 J. Lienig, Presented at SLIP'05 International workshop on system level interconnect prediction, San Francisco, California, U.S.A., April, 2005.
4 J. R. Black, *IEEE Trans. Electron Devices*, 1969, **16**, 338.
5 ITRS International Technology Working Groups, International Technology Roadmap for Semiconductors, http://www.itrs.net, accessed May, 2015.
6 (*a*) P. S. Ho and T. Kwok, *Rep. Prog. Phys.*, 1989, **52**, 301; (*b*) P. C. Li and T. K. Young, *IEEE Spectrum*, 1996, **33**, 75; (*c*) L. Pauling, *The Nature of Chemical Bond*, Cornell University Press, USA, 1960.
7 S. Krishnan, S. V. Garimella, G. M. Chrysler and R. V. Mahajan, *IEEE Trans. Adv. Pack.*, 2007, **30**, 462.
8 (*a*) Z. Yao, C. L. Kane and C. Dekker, *Phys. Rev. Lett.*, 2000, **84**, 2941; (*b*) B. Q. Wei, R. Vajtai and P. M. Ajayan, *Appl. Phys. Lett.*, 2001, **79**, 1172; P. G. Collins, M. Hersam, M. Arnold, R. Martel and P. H. Avouris, *Phys. Rev. Lett.*, 2001, **86**, 3128; (*c*) X. Wang, N. Behabtu, C. C. Young, D. E. Tsentalovich, M. Pasquali and J. Kono, *Adv. Funct. Mater.*, 2014, **24**, 3241; (*d*) D. Janas, A. P. Herman, S. Boncel and K. K. K. Koziol, *Carbon*, 2014, **73**, 225.
9 (*a*) R. Murali, Y. Yang, K. Brenner, T. Beck and J. D. Meindl, *Appl. Phys. Lett.*, 2009, **94**, 243114; (*b*) K. J. Lee, A. P. Chandrakasan and K. Jing, *IEEE Electron Device Lett.*, 2011, **32**, 557; (*c*) A. D. Liao, J. Z. Wu, X. Wang, K. Tahy, D. Jena, H. Dai and E. Pop, *Phys. Rev. Lett.*, 2011, **106**, 256801.
10 C. Subramaniam, T. Yamada, K. Kobashi, A. Sekiguchi, D. N. Futaba, M. Yumura and K. Hata, *Nat. Commun.*, 2013, **4**, 2202.
11 C. Subramaniam, Y. Yasuda, S. Takeya, S. Ata, A. Nishizawa, D. Futaba, T. Yamada and K. Hata, *Nanoscale*, 2014, **6**, 2669.
12 K. Hata, D. N. Futaba, K. Mizuno, T. Namai, M. Yumura and S. Iijima, *Science*, 2004, **306**, 1362.
13 (*a*) Y. Hayamizu, T. Yamada, K. Mizuno, R. C. Davis, D. N. Futaba, M. Yumura and K. Hata, *Nat. Nanotechnol.*, 2008, **3**, 289; (*b*) T. Yamada, Y. Hayamizu, Y. Yamamoto, Y. Yomogida, A. I. Najafabadi, D. N. Futaba and K. Hata, *Nat. Nanotechnol.*, 2011, **6**, 296; (*c*) T. Yamada, N. Makimoto, A. Sekiguchi, Y. Yamamoto, K. Kobashi, Y. Hayamizu, Y. Yomogida, H. Tanaka, H. Shima, H. Akinaga, D. Futaba and K. Hata, *Nano Lett.*, 2012, **12**, 4540; (*d*) T. Yamada, Y. Yamamoto, Y. Hayamizu, A. Sekiguchi, H. Tanaka, K. Kobashi, D. N. Futaba and K. Hata, *ACS Nano*, 2013, **7**, 3177.
14 S. D. Bergin, Z. Sun, D. Rickard, P. V. Streich, J. P. Hamilton and J. N. Coleman, *ACS Nano*, 2009, **3**, 2340.
15 A. Vassighi and M. Sachdev, *IEEE Trans. Device Mater. Reliab.*, 2006, **6**, 300.
16 S. Savastiouk, *Solid State Technol.*, 2000, **43**, 84.
17 L. G. Gosset, A. Farcy, J. de Pontcharra, Ph. Lyan, R. Daamen, G. J. A. M. Verheijden, V. Arnal, F. Gaillard, D. Bouchu, P. H. L. Bancken, T. Vandeweyer, J. Michelon, V. N. Hoang, R. J. O. M. Hoofman and J. Torres, *Microelectron Eng.*, 2005, **82**, 321.
18 (*a*) J. R. Black, *IEEE Trans. Electron Devices*, 1969, **16**, 338; (*b*) J. R. Lloyd, *J. Appl. Phys.*, 1991, **69**, 7601.
19 (*a*) C. L. Liu, *Appl. Phys. Lett.*, 2002, **80**, 763; (*b*) C. L. Liu, X. Y. Liu and L. J. Borucki, *Appl. Phys. Lett.*, 1999, **74**, 34; (*c*) C. L. Liu, *Phys. Status Solidi*, 2001, **1**, 47; (*d*) P. Wilhite, A. A. Vyas, J. Tan, J. Tan, T. Yamada, P. Wang, J. Park and C. Y. Yang, *Semicond. Sci. Technol.*, 2014, **29**, 054006; (*e*) M. G-Asl, P. D. Bristowe and K. Koziol, *Phys. Chem. Chem. Phys.*, 2015, **17**, 18273.